

Nitrogen-Atom Transfer from $[PW_{11}O_{39}Ru^VI N]^{4-}$ to PPh_3

Claire Besson,^{†,‡} Yurii V. Geletii,[‡] Françoise Villain,^{†,§} Richard Villanneau,[†] Craig L. Hill,[‡] and Anna Proust^{*,†,||}

[†]*Institut parisien de chimie moléculaire, UMR 7071, Case courrier 42, UPMC univ Paris 06, 4 place Jussieu, 75252 Paris Cedex, France,* [‡]*Department of Chemistry, Emory University, Atlanta, Georgia 30322, and*

[§]*Synchrotron SOLEIL, l'Orme des Merisiers, Saint-Aubin BP 48, 91192 Gif sur Yvette, France.* ^{||}*Member of IUF.*

Received July 10, 2009

The nitrido derivative $(n-Bu_4N)_4[PW_{11}O_{39}Ru^VI N]$ transfers its nitrogen atom to triphenylphosphine to give quantitatively the bis(triphenylphosphane)iminium cation $[Ph_3PNPPh_3]^+$. An intermediate can be prepared by the reaction of a single molecule of triphenylphosphine with the polyoxometalate, the iminophosphorane derivative $(n-Bu_4N)_3-[PW_{11}O_{39}Ru^V\{NPPH_3\}]$. The reactivity of the latter species has been investigated to complete the general scheme of the nitrogen-transfer reaction. By the addition of 1 equiv of hydroxide, $[PW_{11}O_{39}Ru^{III}\{N(OH)PPh_3\}]^{4-}$ is obtained. The reaction can be reversed by the addition of one proton. The phosphinoxime derivative $[PW_{11}O_{39}Ru^{III}\{N(OH)PPh_3\}]^{4-}$ can be prepared in solution but is unstable. It decomposes to yield quantitatively $(n-Bu_4N)_4[PW_{11}O_{39}Ru^{III}\{OPPh_3\}]$. All of those species have been thoroughly characterized by mass spectrometry, paramagnetic ³¹P NMR, IR, Raman, UV–visible, XANES, and EXAFS spectroscopies.

Introduction

The chemistry of ruthenium encompasses a wide range of reactions,¹ such as olefin metathesis,² solar energy conversion,³ and atom transfer,^{4,5} to cite only a few examples. In the latter case, as in most oxidation catalysts, one of the significant problems encountered is the degradation of the ligand and subsequent loss of activity of the catalyst.

Lacunary polyoxometalates (POMs), i.e., POMs formally lacking metallic centers, are a class of all-inorganic ligands with a set of properties, e.g., multidenticity, rigidity, and hydrolytical (providing pH control), thermal and oxidative stability, which make them quite attractive for oxidation catalysis.^{6–8} In particular, the past decade has witnessed growing interest for the incorporation of noble-metal cations

into POMs⁹ and has underlined the unique ability of POMs to stabilize transition-metal cations with high oxidation states.^{10–13} A similar quest for high-oxidation-state ruthenium-containing POMs^{14,15} has very recently come to a head with the report of an adamantane-like Ru^{IV} tetramer stabilized by two divacant decatungstosilicates¹⁶ that proved to be catalytically active toward water oxidation.^{17–19} The stabilization of high oxidation states should be easier with the more π -electron-donating nitrido ligands, and indeed $[PW_{11}O_{39}RuN]^{4-}$ (1) formally includes a Ru^{VI} center, from which we

*To whom correspondence should be addressed. E-mail: anna.proust@upmc.fr.

(1) Naota, T.; Takaya, H.; Murahashi, S.-I. *Chem. Rev.* 1998, 98, 2599–2660.

(2) Grubbs, R. H. *Angew. Chem., Int. Ed.* 2006, 45, 3760–3765.

(3) Liu, F.; Concepcion, J. J.; Jurss, J. W.; Cardolaccia, T.; Templeton, J. L.; Meyer, T. J. *Inorg. Chem.* 2008, 47, 1727–1752.

(4) Leung, S. K.-Y.; Huang, J.-S.; Liang, J.-L.; Che, C.-M.; Zhou, Z.-Y. *Angew. Chem., Int. Ed.* 2003, 42, 340–343.

(5) Man, W.-L.; Lam, W. W. Y.; Yiu, S.-M.; Lau, T.-C.; Peng, S.-M. *J. Am. Chem. Soc.* 2004, 126, 15336–15337.

(6) Hill, C. L.; Prosser-McCartha, C. M. *Coord. Chem. Rev.* 1995, 143, 407–455.

(7) Neumann, R. *Prog. Inorg. Chem.* 1998, 47, 317–370.

(8) Mizuno, N.; Yamaguchi, K.; Kamata, K. *Coord. Chem. Rev.* 2005, 249, 1944–1956.

(9) Bi, L.-H.; Reike, M.; Kortz, U.; Keita, B.; Nadjó, L.; Clark, R. J. *Inorg. Chem.* 2004, 43, 3915–3920.

(10) Anderson, T. M.; Neiwert, W. A.; Kirk, M. L.; Piccoli, P. M. B.; Schultz, A. J.; Koetzle, T. F.; Musaev, D. G.; Morokuma, K.; Cao, R.; Hill, C. L. *Science* 2004, 306, 2074–2077.

(11) Anderson, T. M.; Cao, R.; Slonkina, E.; Hedman, B.; Hodgson, K. O.; Hardcastle, K. I.; Neiwert, W. A.; Wu, S. X.; Kirk, M. L.; Knottenbelt, S.; Depperman, E. C.; Keita, B.; Nadjó, L.; Musaev, D. G.; Morokuma, K.; Hill, C. L. *J. Am. Chem. Soc.* 2005, 127, 11948–11949.

(12) Cao, R.; Anderson, T. M.; Piccoli, P. M. B.; Schultz, A. J.; Koetzle, T. F.; Geletii, Y. V.; Slonkina, E.; Hedman, B.; Hodgson, K. O.; Hardcastle, K. I.; Fang, X.; Kirk, M. L.; Knottenbelt, S.; Kögerler, P.; Musaev, D. G.; Morokuma, K.; Takahashi, M.; Hill, C. L. *J. Am. Chem. Soc.* 2007, 129, 11118–11133.

(13) Khenkin, A. M.; Kumar, D.; Shaik, S.; Neumann, R. *J. Am. Chem. Soc.* 2006, 128, 15451–15460; 2007, 129, 723.

(14) Randall, W. J.; Weakley, T. J. R.; Finke, R. G. *Inorg. Chem.* 1993, 32, 1068–1071.

(15) Chen, S.-W.; Villanneau, R.; Li, Y.; Chamoiseau, L.-M.; Boubekeur, K.; Thouvenot, R.; Gouzerh, P.; Proust, A. *Eur. J. Inorg. Chem.* 2008, 2137–2142.

(16) Yamaguchi, S.; Uehara, K.; Kamata, K.; Yamaguchi, K.; Mizuno, N. *Chem. Lett.* 2008, 37, 328–329.

(17) Geletii, Y. V.; Botar, B.; Kögerler, P.; Hillesheim, D. A.; Musaev, D. G.; Hill, C. L. *Angew. Chem., Int. Ed.* 2008, 47, 3896–3899.

(18) Sartorel, A.; Carraro, M.; Scorrano, G.; Zorzi, R. D.; Geremia, S.; McDaniel, N. D.; Bernhard, S.; Bonchio, M. *J. Am. Chem. Soc.* 2008, 130, 5006–5007.

(19) Geletii, Y. V.; Huang, Z.; Hou, Y.; Musaev, D. G.; Lian, T.; Hill, C. L. *J. Am. Chem. Soc.* 2009, 131, 7522–7523.

evidenced the first nitrogen-atom transfer from a functionalized POM.²⁰ We present here a more detailed analysis of the reactivity of the iminophosphorane $[\text{PW}_{11}\text{O}_{39}\text{Ru}^{\text{V}}\{\text{NPPH}_3\}]^{3-}$ (**2**). Very little is known about the reactivity of iminophosphorane complexes in general,^{21,22} and almost nothing is known in the case of ruthenium.²³ Our contribution also provides spectroscopic characterization of ruthenium in various oxidation states in the POM, which might be useful to elucidate the reaction mechanisms of ruthenium-containing POMs. This will complete the analytical data gathered in the seminal article by Pope et al. in 1992²⁴ and more recent papers from Sadakane et al.^{25–27}

Experimental Section

Instrumentation and Techniques of Measurement. IR spectra were recorded from KBr pellets (dilution of approximately 2% in weight) on a Bio-Rad Win-IR FTS 165 FT-IR spectrophotometer. Raman spectra were recorded on a Kaiser Optica Systems HL5R spectrometer equipped with a near-IR laser diode working at 785 nm. The laser power was set to 8 mW. Solid samples were used for all compounds, except for $(n\text{-Bu}_4\text{N})_4[\text{PW}_{11}\text{O}_{39}\text{Ru}^{\text{III}}\{\text{N}(\text{OH})\text{PPh}_3\}] [(n\text{-Bu}_4\text{N})_4(\mathbf{3})]$. In the latter case, a 4.4 mM solution in acetonitrile was used. UV–visible spectra were acquired on an Agilent 8453 UV–visible spectroscopy system or on a Shimadzu UV-2101 spectrophotometer and, for fast kinetics, on a High-Tech SF-61SX2 stopped-flow system equipped with a Bentham M300 monochromator. Kinetic data analysis was performed using *Gepasi* software²⁸ for numerical integration and fit. The ³¹P (121.5 MHz), ¹³C (75.6 MHz), and ¹H (300 MHz) NMR spectra were obtained at 300 K in 5-mm-o.d. tubes on a Bruker Avance II 300 spectrometer equipped with a QNP probehead. The chemical shifts are given with respect to 85% H₃PO₄ for ³¹P NMR (measured by the substitution method) and with respect to tetramethylsilane for ¹H NMR (using a nondeuterated solvent as an internal secondary reference) and ¹³C NMR (using the solvent peaks as an internal secondary reference). Cyclic voltammetry (CV) studies were performed in an acetonitrile solution with an EG&G model 273A system using a standard three-electrode cell. The working electrode is a glassy carbon electrode (diameter 3 mm), the reference electrode is a calomel electrode (CE) filled with a 3 M LiCl solution and equipped with a double junction, and the counter electrode is a platinum wire. The electrolyte is $(n\text{-Bu}_4\text{N})\text{BF}_4$ (0.1 M), and the scan rate is 100 mV·s⁻¹ unless otherwise noted. All potentials are given relative to the CE. Electrospray ionization mass spectrometry (ESI-MS) spectra were recorded using an ion-trap mass spectrometer (Bruker Esquire 3000) equipped with an orthogonal ESI-MS source. Sample solutions (50 μM in acetonitrile) were injected into the ESI-MS source using a syringe pump with a flow rate of 120 μL·min⁻¹. The capillary high voltage was set to 3500 V. The capillary exit and first skimmer were varied between -18.0 and -45.0 V for the former and between -8.0 and -15.0 V

for the latter, in order to identify peaks due to in-source decomposition.

Synthesis. $\text{K}_7[\text{PW}_{11}\text{O}_{39}] \cdot 14\text{H}_2\text{O}$,²⁹ $(n\text{-Bu}_4\text{N})[\text{Ru}^{\text{VI}}\text{NCl}_4]$,³⁰ $(n\text{-Bu}_4\text{N})_4[\text{PW}_{11}\text{O}_{39}\text{Ru}^{\text{VI}}\text{N}] [(n\text{-Bu}_4\text{N})_4(\mathbf{1})]$ ²⁰ were prepared following published procedures; their purities were checked by IR spectroscopy and, when applicable, by ¹H or ³¹P NMR spectroscopy. Reagent-grade solvents and reagents were used as received unless specifically indicated. $(n\text{-Bu}_4\text{N})\text{OH}$ (initially 40% by weight in methanol) was titrated by 0.1 M HCl in water before use.

$(n\text{-Bu}_4\text{N})_3[\text{PW}_{11}\text{O}_{39}\text{Ru}^{\text{V}}\{\text{NPPH}_3\}] [(n\text{-Bu}_4\text{N})_3(\mathbf{2})]$. Compound **2** was prepared by a modification of the previously published procedure.²⁰ To a green solution of $(n\text{-Bu}_4\text{N})_4(\mathbf{1})$ (665 mg in 15 mL of CH₃CN, 0.18 mmol) was slowly added a 1:1 mixture of PPh₃ (48 mg, 0.18 mmol) and *p*-toluenesulfonic acid monohydrate (33 mg, 0.18 mmol) dissolved in 5 mL of CH₃CN. The resulting orange solution was poured into 200 mL of diethyl ether under agitation, yielding an orange precipitate. Purification was achieved by column chromatography using a 10-cm-wide column, 850 mL of wet silica gel 60 (0.063–0.200 nm particle size), and a 1:1 mixture of acetonitrile and methylene chloride as the eluent. The first orange fraction was evaporated to dryness by rotary evaporation at 35 °C, yielding 580 mg (84%) of $(n\text{-Bu}_4\text{N})_3(\mathbf{2})$ as a red-orange powder. IR (KBr) ν_{max} (cm⁻¹): 388 (s), 518 (m), 690 (w), 724 (w), 806 (vs), 886 (s), 969 (s), 1049 (m), 1087 (s), 1114 (w), 1381 (w), 1438 (w), 1484 (m), 2874 (w), 2833 (w), 2962 (m). Raman ν_{max} (cm⁻¹): 165 (m), 213 (m), 227 (w), 252 (w), 528 (m), 661 (m), 900 (m), 988 (vs), 1027 (w), 1103 (w), 1318 (w), 1449 (w), 1588 (w), 2892 (w). UV [CH₃CN; λ_{max} , nm (log ϵ): 442 (3.7)]. ³¹P NMR (121.5 MHz, CD₃CN, 300 K): δ (ppm) 322 ($\Delta\nu_{1/2}$ = 90 Hz). ¹H NMR (300.13 MHz, CD₃CN, 300 K): δ (ppm) 1.00 (t, 36H, (CH₃(CH₂)₃)₄N⁺), 1.41 (h, 24H, (CH₃CH₂(CH₂)₂)₄N⁺), 1.67 (m, 24H, (CH₃CH₂CH₂CH₂)₄N⁺), 3.16 (m, 24H, (CH₃(CH₂)₂CH₂)₄N⁺), 7.57 (t, *J* = 7.0 Hz, 3H, *p*-C₆H₅), 9.44 (d, *J* = 5.6 Hz, 6H, *m*-C₆H₅), 12.05 (br, $\Delta\nu_{1/2}$ = 25 Hz, 6H, *o*-C₆H₅). ¹³C NMR (75.6 MHz, CD₃CN, 300 K): δ (ppm) 14.1, 20.7, 24.7, 59.7, 143.9, 147.9, 190.3. ESI-MS: *m/z* (Da) 931 ([2 - PPh₃]³⁻, in situ degradation), 1018 ([2]³⁻), 1528 ([H2]²⁻), 1649 [(*n*-Bu₄N)**2**]²⁻. CV [*E*_{1/2}, mV vs CE in CH₃CN ($\Delta E_{1/2}$, mV)]: -713 (122), 311 (73). EPR:²⁰ $g_1 = 2.51$, $g_2 = 2.32$, $g_3 = 1.68$.

$(n\text{-Bu}_4\text{N})_4[\text{PW}_{11}\text{O}_{39}\text{Ru}^{\text{III}}\{\text{N}(\text{OH})\text{PPh}_3\}] [(n\text{-Bu}_4\text{N})_4(\mathbf{3})]$. Compound **3** can be prepared by the careful addition of $(n\text{-Bu}_4\text{N})\text{OH}$ to a solution of $(n\text{-Bu}_4\text{N})_3(\mathbf{2})$ monitored by ³¹P NMR and UV–visible spectroscopy. The synthesis from $(n\text{-Bu}_4\text{N})_4(\mathbf{1})$ described below, however, allows skipping of the lengthy chromatography step involved in the preparation of **2**. Also, the smaller amount of $(n\text{-Bu}_4\text{N})\text{OH}$ added makes the solution of **3** more stable. A green solution of **1** was prepared by dissolution of 250 mg (66 μmol) of $(n\text{-Bu}_4\text{N})_4(\mathbf{1})$ in 10 mL of CH₃CN freshly distilled over CaH₂ and cooled to 0 °C in an ice bath. To this vigorously stirred solution was added via a dropping funnel (1 drop every 10 s) 5 mL of a solution of PPh₃ (13.3 mM, 66 μmol) and $(n\text{-Bu}_4\text{N})\text{OH}$ (7.32 mM, 37 μmol) prepared from PPh₃, a $(n\text{-Bu}_4\text{N})\text{OH}$ stock solution, and freshly distilled acetonitrile. If the presence of $(n\text{-Bu}_4\text{N})_3(\mathbf{2})$ is detected by ³¹P NMR, an extra amount of $(n\text{-Bu}_4\text{N})\text{OH}$ can be carefully added, until only the desired product is present. This solution of **3** (4.4 mM; no impurity detected by ³¹P NMR) can be stored for months at liquid-nitrogen temperature but decomposes in a few hours at room temperature. Raman (4.4 mM in acetonitrile, cm⁻¹): ν_{max} 600 (br, m), 799 (m), 830 (w), 877 (w), 978 (m), 996 (w), 1036 (w), 2116 (m). UV [CH₃CN; λ_{max} , nm (log ϵ): 405 (4.1)]. ³¹P NMR (121.5 MHz, CD₃CN, 300 K): δ (ppm) 449 ($\Delta\nu_{1/2}$ = 90 Hz). ¹H NMR (300.13 MHz, CD₃CN, 300 K): δ (ppm) 9.82, ($\Delta\nu_{1/2}$ = 17 Hz),

(29) Contant, R. *Can. J. Chem.* **1987**, *65*, 568–573.

(30) Griffith, W. P.; Pawson, D. *J. Chem. Soc., Dalton Trans.* **1973**, 1315–1320.

(20) Lahootun, V.; Besson, C.; Villanneau, R.; Villain, F.; Chamoreau, L.-M.; Boubekeur, K.; Blanchard, S.; Thouvenot, R.; Proust, A. *J. Am. Chem. Soc.* **2007**, *129*, 7127–7135.

(21) Dehnicke, K.; Krieger, M.; Massa, W. *Coord. Chem. Rev.* **1999**, *182*, 19–65.

(22) Demadis, K. D.; Bakir, M.; Kleszczewski, B. G.; Williams, D. S.; White, P. S.; Meyer, T. J. *Inorg. Chim. Acta* **1998**, *270*, 511–526.

(23) Chan, P.-M.; Yu, W.-Y.; Che, C.-M.; Cheung, K.-K. *J. Chem. Soc., Dalton Trans.* **1998**, 3183–3190.

(24) Rong, C.; Pope, M. T. *J. Am. Chem. Soc.* **1992**, *114*, 2932–2938.

(25) Sadakane, M.; Higashijima, M. *Dalton Trans.* **2003**, 659–664.

(26) Sadakane, M.; Tsukuma, D.; Dickman, M. H.; Bassil, B. S.; Kortz, U.; Higashijima, M.; Ueda, W. *Dalton Trans.* **2006**, 35, 4271–4276.

(27) Sadakane, M.; Tsukuma, D.; Dickman, M. H.; Bassil, B. S.; Kortz, U.; Capron, M.; Ueda, X. *Dalton Trans.* **2007**, 2833–2838.

(28) Mendes, P. *Gepasi v. 3.0. Comput. Appl. Biosci.* **1993**, *9*, 563–571.

19.2 ($\Delta\nu_{1/2} = 15$ Hz). MS: m/z (Da) 947 ($[\text{H}_3 - \text{PPh}_3]^{3-}$, in situ degradation), 1024 ($[\text{H}_3]^{3-}$), 1105 ($[(n\text{-Bu}_4\text{N})_3]^{3-}$), 1778 ($[(n\text{-Bu}_4\text{-N})_2]^{3-}$).

($n\text{-Bu}_4\text{N}$)₄[PW₁₁O₃₉Ru^{III}{OPPh₃}] [($n\text{-Bu}_4\text{N}$)₄(4)]. Compound **4** forms quantitatively when a solution of **3** (see above) is allowed to sit at room temperature. However, completion of the reaction, as determined by ³¹P NMR, is achieved after 1 or 2 days only. Alternatively, a solution of **4** can be prepared more rapidly from the solution of **3** obtained above by the addition of ($n\text{-Bu}_4\text{N}$)OH: 15 mL of the 4.4 mM solution of **3** (66 μmol) was brought back to room temperature, and 0.52 mL of a 127 mM ($n\text{-Bu}_4\text{N}$)OH solution, prepared by dilution in acetonitrile of the commercial stock solution (66 μmol , 1 equiv), was then added in 0.05 mL portions. The solution turned from deep orange to dark brown. The addition of 30 mL of diethyl ether induced the precipitation of 200 mg of ($n\text{-Bu}_4\text{N}$)₄(**4**) (75% yield based on the initial ($n\text{-Bu}_4\text{N}$)₄[PW₁₁O₃₉Ru^{VI}N]). Brown cubic crystals of ($n\text{-Bu}_4\text{N}$)₄(**4**) (160 mg, 60% yield based on the initial ($n\text{-Bu}_4\text{N}$)₄[PW₁₁O₃₉Ru^{VI}N]) were grown in 2 days from an acetonitrile solution under diethyl ether diffusion. IR (KBr, cm^{-1}): ν_{max} 377 (s), 495 (m), 516 (m), 588(s), 693 (w), 721 (w), 784 (vs), 801 (vs), 877 (s), 957 (s), 1002 (w), 1041 (m), 1078 (s), 1112 (w), 1152 (w), 1381 (w), 1438 (w), 1484 (m), 2874 (w), 2935 (w), 2962 (m). Raman (cm^{-1}): ν_{max} 212 (m), 236 (m), 335 (w), 380 (m), 468 (m), 498 (m), 687 (w), 797 (s), 872 (s), 961 (vs), 975 (vs), 1000 (m), 1029 (m), 1040 (m), 1105 (m), 1318 (w), 1460 (w), 1590 (w), 2892 (m). UV [CH_3CN ; λ_{max} , nm (log ϵ): 360 (3.9)]. ³¹P NMR (121.5 MHz, CD_3CN , 300 K): δ (ppm) -400 ($\Delta\nu_{1/2} = 875$ Hz), 190 ($\Delta\nu_{1/2} = 270$ Hz). ¹H NMR (300.13 MHz, CD_3CN , 300 K): δ (ppm) 1.02 (t, 48H, ($\text{CH}_3(\text{CH}_2)_3\text{N}^+$), 1.44 (h, 32H, ($\text{CH}_3\text{CH}_2(\text{CH}_2)_2\text{N}^+$), 1.68 (m, 32H, ($\text{CH}_3\text{CH}_2\text{CH}_2\text{CH}_2\text{N}^+$), 3.19 (m, 32H, ($\text{CH}_3(\text{CH}_2)_2\text{CH}_2\text{N}^+$), 7.55 (t, $J = 5.9$ Hz, 3H, $p\text{-C}_6\text{H}_5$), 7.73 (br, $\Delta\nu_{1/2} = 50$ Hz, 6H, $o\text{-C}_6\text{H}_5$), 8.90 (d, $J = 5.7$ Hz, 6H, $m\text{-C}_6\text{H}_5$). ESI-MS: m/z (Da) 932 ($[\text{H}_4 - \text{PPh}_3]^{3-}$, in situ degradation), 1019 ($[\text{H}_4]^{3-}$), 1650 ($[(n\text{-Bu}_4\text{N})_4]^{2-}$), 1771 ($[(n\text{-Bu}_4\text{N})_2]^{2-}$). Crystallographic data: cubic, space group $I43m$, $a = 17.59$ Å, $V = 5440$ Å³.

($n\text{-Bu}_4\text{N}$)₄[PW₁₁O₃₉Ru^{III}{OH₂}] [($n\text{-Bu}_4\text{N}$)₄(5)]. This compound was prepared using Rong and Pope's synthesis,²⁴ except that $[\text{Ru}^{\text{II}}(\text{DMF})_6](\text{OSO}_3\text{CF}_3)_2$ (DMF = N,N -dimethylformamide) was used instead of $[\text{Ru}^{\text{II}}(\text{OH}_2)_6](\text{OSO}_3\text{CF}_3)_2$ for the preparation of the intermediate $\text{Cs}_4[\text{PW}_{11}\text{O}_{39}\text{Ru}^{\text{III}}\{\text{OH}_2\}]$. IR (KBr) (cm^{-1}): ν_{max} 374 (m), 390 (m), 513 (w), 800 (vs), 883 (s), 961 (s), 1047 (m), 1082 (s), 1381 (m), 1484 (s), 2876 (s), 2937 (m), 2963 (s). Raman (cm^{-1}): ν_{max} 212 (m), 225 (m), 310 (w), 323 (m), 800 (m), 878 (m), 970 (sh), 979 (s), 1043 (w), 1130 (w), 1460 (w), 2285 (m), 2892 (m). UV [CH_3CN ; λ_{max} , nm (log ϵ): 360 (3.3)]. ³¹P NMR (121.5 MHz, CD_3CN , 300 K): δ (ppm) -70 ($\Delta\nu_{1/2} = 1000$ Hz).²⁴ CV [$E_{1/2}$, mV vs SCE in CH_3CN ($\Delta E_{1/2}$, mV): -1600 (100), -240 (80), 950 (300)].

Reaction of ($n\text{-Bu}_4\text{N}$)₃(2) with PPh₃. To an orange solution of ($n\text{-Bu}_4\text{N}$)₃(**2**) (28.3 mg in 2 mL of CH_3CN , 7.5 μmol) were successively added 1 mL of a 29 mM solution of p -toluenesulfonic acid (29 μmol) and 1 mL of a 7.5 mM solution of PPh₃ (7.5 μmol). The solution slowly turned brown. The sole products detected by ³¹P NMR after 3 days of reaction were $[\text{Ph}_3\text{PNPPH}_3]^+$ (δ 22 ppm) and **5** (δ -70 ppm).

X-ray Absorption Spectroscopies. X-ray absorption near-edge spectroscopy (XANES) and extended X-ray absorption fine structure spectroscopy (EXAFS) data were obtained at the Soleil synchrotron source, on the SAMBA beamline. The spectra were recorded at the Ru K-edge (22 117 eV). Detection in transmission mode at liquid-nitrogen temperature was used for solid samples ground and pressed into a pellet. Spectra of ($n\text{-Bu}_4\text{N}$)₄(**3**) as a frozen acetonitrile solution (4.4 mM, i.e., about 400 ppm weight in ruthenium) were recorded at liquid-

nitrogen temperature with fluorescence detection. The experiments were calibrated with a foil of metallic ruthenium. After background correction, the XANES spectra were normalized at 22 230 eV. The EXAFS analysis was performed using the "EXAFS pour le MAC" package.³² The EXAFS signal was extracted from the raw data by subtracting a linear pre-edge background and normalized by the Lengeler–Eisenberger procedure.³³ The pseudoradial distribution was given by the Fourier transform of $\omega(k)k^3\chi(k)$, where $\chi(k)$ is a Kaiser–Bessel window with a smoothness parameter equal to 3. The k limits are 2.8 and 12.1 Å⁻¹. A single scattering fit of experimental curves was performed with the *RoundMidnight* program³⁴ with ab initio amplitude and phase functions calculated in ($n\text{-Bu}_4\text{N}$)₃(**2**) using the FEFF7 code.³⁵ The FEFF7 code was also used to calculate the theoretical absorption spectrum for ($n\text{-Bu}_4\text{N}$)₃(**2**) using the structure determined by X-ray diffraction. A marginal improvement of the fit between the calculated and experimental spectra was observed when double scattering was used instead of simple scattering. Longer scattering paths did not improve the results.

Results

Interest in metal–nitrido and metal–imido complexes stems from their general relevance to dinitrogen activation, on the one hand,³⁶ and their potential role in C–N bond formation, on the other hand.^{4,5,37–41} Ruthenium nitrido complexes have been far less studied than their osmium analogues,^{22,42,43} although the reactivity of the {RuN} function appears to be more dependent upon the ancillary ligands.^{43,44} However, this function is generally expected to be electrophilic,⁴⁵ as we have indeed verified. Following the report of our preliminary results,²⁰ we present here a more comprehensive study of the reactivity of complexes ($n\text{-Bu}_4\text{N}$)₄(**1**) and ($n\text{-Bu}_4\text{N}$)₃(**2**).

Reaction of $[\text{PW}_{11}\text{O}_{39}\text{Ru}^{\text{VI}}\text{N}]^{4-}$ with PPh₃. The reaction of **1** with 1 equiv of triphenylphosphine in acetonitrile, monitored by ³¹P NMR, yields a mixture of two species: **2** and **3**. The isolation and characterization of the former has been described in a previous paper.²⁰ We noticed that the yield of **2** after separation by chromatography on a silica column (70%) was higher than expected, while any trace of **3** disappeared. This prompted us to investigate the acid–base reactivity of those species. Indeed, **3** is cleanly converted to **2** by the addition of 1 equiv of a

(32) Michalowicz, A. EXAFS version 1998 pour Mac OS9, http://www.univ-paris12.fr/40615508/0/fiche_3000A_pagelibre/.

(33) Lengeler, B.; Eisenberg, P. *Phys. Rev. B* **1980**, *21*, 4507.

(34) Michalowicz, A. RoundMidnight pour Mac OSX, http://www.univ-paris12.fr/40615508/0/fiche_3000A_pagelibre/.

(35) Zabinsky, S. I.; Rehr, J. J.; Ankudinov, J. J.; Albers, R. C.; Eller, M. J. *Phys. Rev. B* **1995**, *52*, 2995–3009.

(36) Schrock, R. R. *Acc. Chem. Res.* **2005**, *38*, 955–962.

(37) Groves, J. T.; Takahashi, T. *J. Am. Chem. Soc.* **1983**, *105*, 2073.

(38) DuBois, J.; Tomooka, C. S.; Hong, J.; Carreira, E. M. *Acc. Chem. Res.* **1997**, *30*, 364.

(39) Ho, C.-M.; Lau, T.-C.; Kwong, H.-L.; Wong, W.-T. *J. Chem. Soc., Dalton Trans.* **1999**, 2411–2414.

(40) Nishimura, M.; Minakata, S.; Thongchant, S.; Ryu, I.; Komatsu, M. *Tetrahedron Lett* **2000**, *41*, 7089–7092.

(41) Au, S.-M.; Huang, J.-S.; Yu, W.-Y.; Fung, W.-H.; Che, C.-M. *J. Am. Chem. Soc.* **1999**, *121*, 9120–9132.

(42) Meyer, T. J.; Huynh, M. H. V. *Inorg. Chem.* **2003**, *42*, 8140–8160.

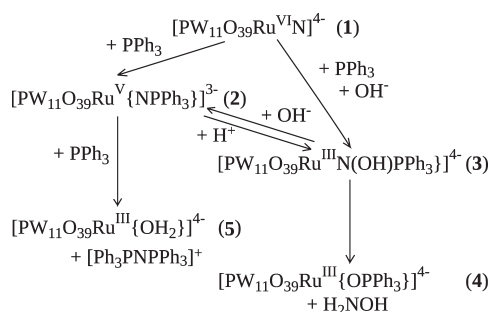
(43) Crevier, T. J.; Bennett, B. K.; Soper, J. D.; Bowman, J. A.; Dehestani, A.; Hrovat, D. A.; Lovell, S.; Kaminsky, W.; Mayer, J. M. *J. Am. Chem. Soc.* **2001**, *123*, 1059–1071.

(44) Sellmann, D.; Wemple, M. W.; Donaubaue, W.; Heinemann, F. W. *Inorg. Chem.* **1997**, *136*, 1397–1402.

(45) Eikey, R. A.; Abu-Omar, M.-M. *Coord. Chem. Rev.* **2003**, *243*, 83–124.

(31) Judd, R. J.; Cao, R.; Biner, M.; Armbruster, T.; Bürgi, H.-B.; Merbach, A. E.; Ludi, A. *Inorg. Chem.* **1995**, *34*, 5080–5083.

Scheme 1



strong acid, thereby explaining our previous observation. Retroconversion of **2** to **3** can be achieved by the addition of 1 equiv of (*n*-Bu₄N)OH or any stronger base (Scheme 1), which led us to formulate **3** as (*n*-Bu₄N)₄[PW₁₁O₃₉Ru^{III}{N(OH)PPh₃}] (for assignment of the ruthenium oxidation state, see below). It should be noted, however, that at variance with what is usually observed in an aqueous solution, the acid–base reactions reported here involve exchange of a hydroxide anion rather than a proton. Regardless of whether a strong base or a sufficient excess of a weaker base such as NEt₃ is used, water inevitably present in the acetonitrile solution quickly yields OH[−] as the reacting species. The concentration of water in acetonitrile can easily reach millimolar concentrations,^{46,47} and even shortly after distillation, there is a 100-fold excess of water over **2** at the low concentration used for UV–visible spectra. The reaction between **2** and OH[−], monitored by stopped flow in the UV–visible range, is first-order with respect to each reagent, with a rate constant of 2 × 10⁶ M^{−1}·s^{−1} at 21 °C. This extremely fast reaction suggests a minimal rearrangement between **2** and **3**. Under the same conditions, the reaction between **3** and *p*-toluenesulfonic acid is completed in less than 2 ms. We could also achieve the selective and direct preparation of either **2** or **3** from **1** by adding PPh₃ in the presence of protons or hydroxides, respectively, under ³¹P NMR monitoring.

The further reaction of [PW₁₁O₃₉Ru^V{NPPH₃}]^{3−} with a second 1 equiv of PPh₃ in an acidic acetonitrile solution yields the bis(triphenylphosphane)iminium cation [Ph₃PNPPH₃]⁺ and [PW₁₁O₃₉Ru^{III}{OH₂}]^{4−} (**5**) as the sole products, identified by their ³¹P NMR chemical shifts compared to those of authentic samples, thus achieving in two steps complete nitrogen-atom transfer from the nitrido polyoxometalate **1** to PPh₃. A similar reaction involving [Os^{IV}(tpy)Cl₂(NPPH₃)]⁺ (tpy = terpyridine) has been reported,²² but an excess of PPh₃ had to be used in that case.

While **2** is stable in solution and in the solid state, its hydroxo derivative, **3**, is hydrolyzed in solution in a matter of minutes to hours, depending on the temperature, the concentration, and the basicity of the solution. This hydrolysis selectively produces a single POM **4** characterized by two broad signals in ³¹P NMR. Alternatively, **4** can be prepared more rapidly by the addition of (*n*-Bu₄N)OH to a solution of **3**, under ³¹P NMR monitoring. We assign this product as (*n*-Bu₄N)₄–

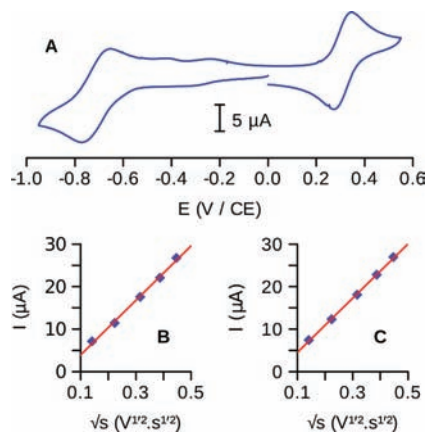


Figure 1. (A) CV of (*n*-Bu₄N)₃(**2**) in CH₃CN at a glassy carbon electrode (rate 100 mV·s^{−1}, calomel reference electrode). (B) Plot of Δ*I* = *i*_{ox} − *i*_{red} as a function of the square root of the scanning speed for the Ru^V/Ru^{IV} couple. (C) Plot of Δ*I* = *i*_{ox} − *i*_{red} as a function of the square root of the scanning speed for the Ru^{VI}/Ru^V couple.

Table 1. ³¹P NMR Chemical Shifts and Half-Widths (CD₃CN, 300 K)

species	1	2	3	4	5 ^a	[Ph ₃ PNPPH ₃] ⁺ ^a
δ _{exp} (ppm)	−13.8	322	449	−400, 190	−70	22
Δν _{1/2} (Hz)	1	90	90	875, 270	1000	0.7

^a Compared to an authentic sample.

[PW₁₁O₃₉Ru^{III}{OPPh₃}] [(*n*-Bu₄N)₄(**4**)], with hydroxylamine as the likely byproduct (cf. Scheme 1). Furthermore, every attempt to precipitate **3** leads to mixtures of **2** and **4** with no or very little **3** present. All studies on **3** were consequently completed in solution.

Oxidation States. The now well-established ability of lacunary POMs to stabilize both high- and low-oxidation-state transition metals was illustrated for ruthenium more than 15 years ago when Rong and Pope isolated and characterized derivatives of the monolacunary polyoxotungstate [PW₁₁O₃₉]^{7−}, with the ruthenium center ranging from Ru^{II} to Ru^{IV}. The oxoruthenium(V) species, though not isolated, was also implicated as an intermediate in oxidation reactions.²⁴ However, the drawback of this versatility of POMs as ligands is that changes of the oxidation state sometimes happen unexpectedly.⁴⁸ According to the literature, one would expect the product of the reaction between [PW₁₁O₃₉Ru^{VI}N]^{4−} and PPh₃ to be a Ru^{IV} species.^{23,49} However, even if phosphorus is indeed oxidized from +III to +V, the oxidation state of ruthenium is decreased by only one unit to yield [PW₁₁O₃₉Ru^V{NPPH₃}]^{3−} as the only product.²⁰ The cyclic voltammogram of **2** displays at 0.31 and −0.71 V/CE two quasi-reversible waves (see Figure 1) that we suggest to attribute respectively to the Ru^{VI}/Ru^V and Ru^V/Ru^{IV} couples because both oxidation states VI and IV are preceded in ruthenium-substituted POMs. Additional waves below −1.20 V/CE mark the first reductions of the tungsten framework, with a possible contribution from a Ru^{IV}/Ru^{III} couple. The values for the Ru^{VI}/Ru^V and Ru^V/Ru^{IV} couples are remarkably

(46) Martin, M. W. In *Recommended method for purification of solvents and tests for impurities*; Coetzee, J. F., Ed.; Pergamon Press: Oxford, U.K., 1982; p 10.

(47) Artero, V. Thèse de l'Université Pierre et Marie Curie, Paris, France, 2000.

(48) Kwen, H.; Tomlinson, S.; Maatta, E. A.; Dablemont, C.; Thouvenot, R.; Proust, A.; Gouzerh, P. *Chem. Commun.* **2002**, 2970–2971.

(49) Yi, X.-Y.; Lam, T. C. H.; Sau, Y.-K.; Zhan, Q.-F.; Williams, I. D.; Leung, W.-H. *Inorg. Chem.* **2007**, *46*, 7193–7198.

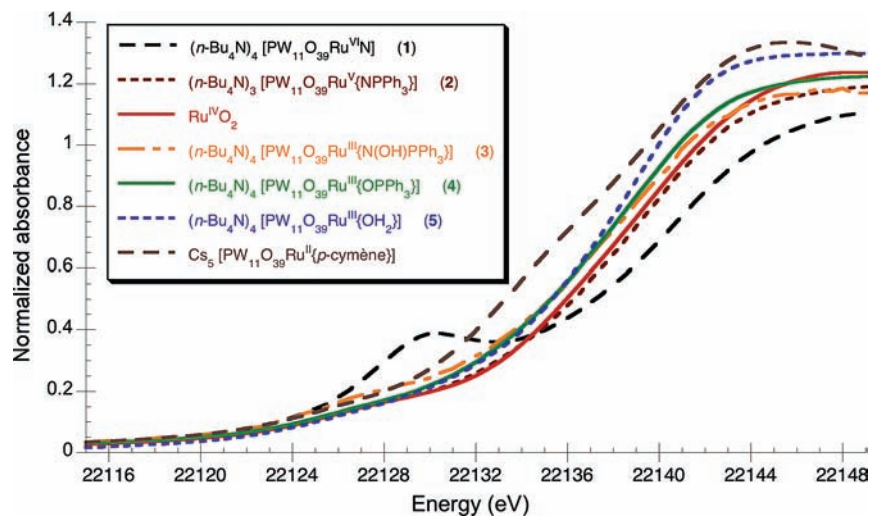


Figure 2. Ru K-edge XANES spectra.

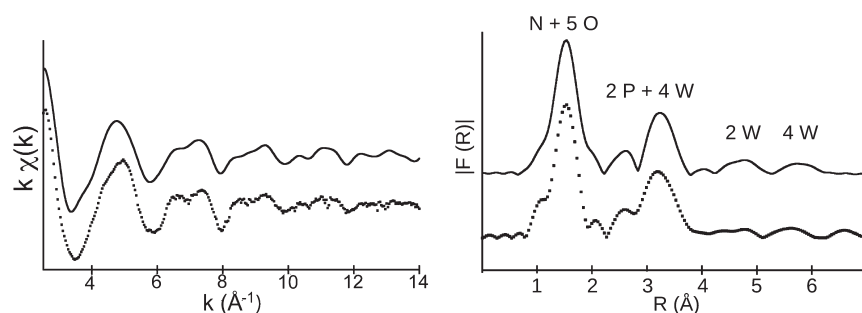


Figure 3. Ru K-edge EXAFS signal of $(n\text{-Bu}_4\text{N})_3(2)$ and its Fourier transform: calculated (solid line) and experimental (dotted line).

low, testifying of the excellent ability of the POM framework to stabilize the high oxidation states of the ruthenium atom. A relatively easy oxidation of the putative intermediate $[\text{PW}_{11}\text{O}_{39}\text{Ru}^{\text{IV}}\{\text{NPPH}_3\}]^{4-}$ is thus expected. The intervention of dioxygen as the potential oxidant, however, can be ruled out because conducting the reaction under argon or dioxygen results in the same products and kinetics. Consequently, one of our main concerns was to reliably identify the ruthenium oxidation state in the different species that we present here.

Our primary tool for assessing the speciation of POMs is ^{31}P NMR, but this technique provides little further information on the oxidation state. Still, the position and width of the peaks (Table 1) are indicative of the magnetic properties of the ruthenium center: diamagnetic (Ru^{VI} in **1** and Ru^{II}) or paramagnetic (Ru^{V} in **2** and Ru^{III} in **3–5**). Further, the NMR data might not always be conclusive because a Ru^{IV} center might be either dia- or paramagnetic.^{5,23,50–52}

XANES at the Ru K-edge is the technique of choice to determine the oxidation state of the metal center. Figure 2 shows the spectra for reference compounds $\text{Cs}_5\text{[PW}_{11}\text{O}_{39}\text{Ru}^{\text{II}}\{p\text{-cymene}\}]$, $(n\text{-Bu}_4\text{N})_4(5)$, $\text{Ru}^{\text{IV}}\text{O}_2$, and $(n\text{-Bu}_4\text{N})_4(1)$ as well as those of $(n\text{-Bu}_4\text{N})_3(2)$, $(n\text{-Bu}_4\text{N})_4(3)$, and $(n\text{-Bu}_4\text{N})_4(4)$. All spectra were recorded in trans-

mission mode on solid samples except for $(n\text{-Bu}_4\text{N})_4(3)$, whose spectrum was registered from a frozen 4.4 mM acetonitrile solution (about 400 ppm of ruthenium in weight) by detection of fluorescence. Because the environment of the ruthenium, a distorted octahedron constituted mainly of oxygen atoms, is similar in all of those species, the position of the edge is expected to be a function of the oxidation state only. The data indicate that this is actually the case, with the energy of the edge increasing as the oxidation state of the ruthenium increases. The edge for **2** lies between the edges of the Ru^{IV} and Ru^{VI} references, thereby confirming the oxidation state of the iminophosphorane derivative as V, in accordance with our previous findings.²⁰ On the other hand, the edges for **3** and **4** are very close to those of **5** and $[\text{Ru}^{\text{III}}(\text{acac})_3]$ ($\text{acac} = \text{acetylacetonate}$, not shown), which indicates that these compounds contain Ru^{III} .

EXAFS. Slow diffusion of ether into an acetonitrile solution of $(n\text{-Bu}_4\text{N})_4(4)$ yields crystals suitable for X-ray diffraction. Unfortunately, they belong to the cubic crystallographic system with the well-known unit cell characterized by $a = 17.59 \text{ \AA}$ and $V = 5440 \text{ \AA}^3$, often encountered in α -Keggin compounds of global charge 4 $^-$, and this precludes any detailed analysis by X-ray diffraction. The asymmetric unit indeed displays only one averaged metallic center composed of $11/12$ tungsten and $1/12$ ruthenium, one disordered terminal ligand, one doubly bridging oxygen, and one quadruply bridging oxygen linked to phosphorus, as previously observed.⁴⁸ The disorder observed in the crystal, however, indirectly

(50) Kuan, S. L.; Tay, E. P. L.; Leong, W. K.; Goh, L. Y.; Lin, C. Y.; Gill, P. M. W.; Webster, R. D. *Organometallics* **2006**, 25, 6134–6141.

(51) Groves, J. T.; Ahn, K.-H. *Inorg. Chem.* **1987**, 26, 3831–3833.

(52) Leung, W.-H.; Hun, T. S. M.; Hou, H.-w.; Wong, K.-Y. *J. Chem. Soc., Dalton Trans.* **1997**, 237–244.

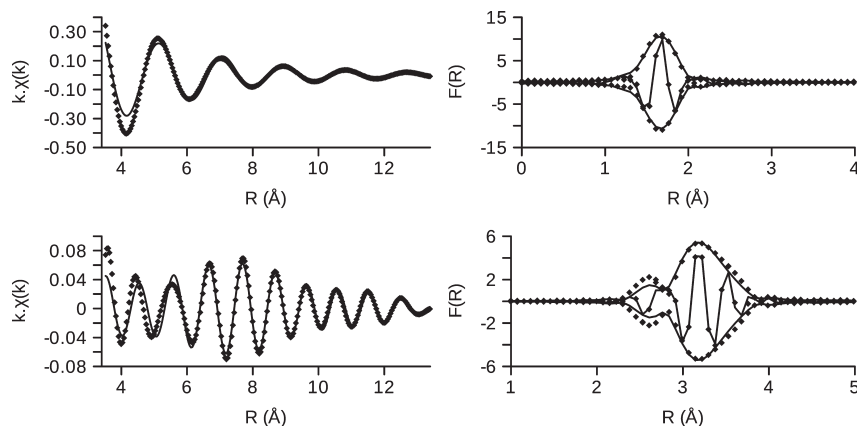


Figure 4. First (above) and second (below) shell filters of the EXAFS spectrum and Fourier transform of $(n\text{-Bu}_4\text{N})_4(4)$: experimental (dotted line) and simulated (solid line).

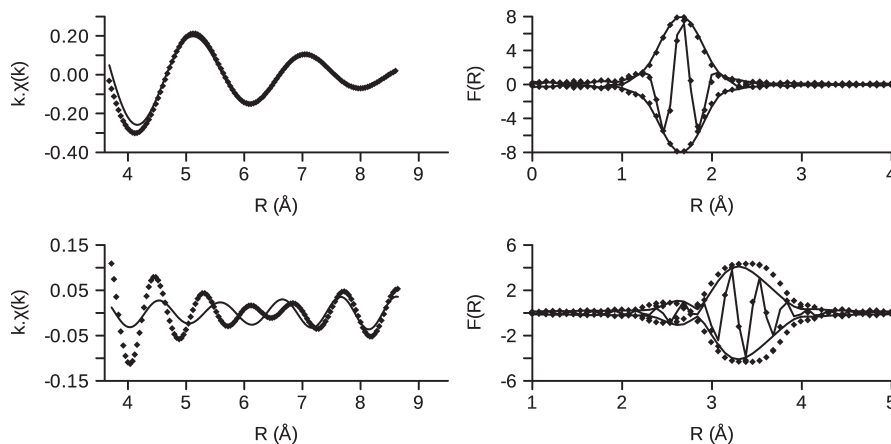


Figure 5. First (above) and second (below) shell filters of the EXAFS spectrum and Fourier transform of $(n\text{-Bu}_4\text{N})_3(3)$: experimental (dotted line) and simulated (solid line). The bad agreement at low k values for the second shell is due to the very low signal-to-noise ratio.

indicates that the ruthenium atom lies in an “in-pocket” position, with the POM framework providing five coordination sites in a fashion similar to that observed in **1**, **2**, and **5**, and not in an “out-of-pocket” position, in which the bonds between the ruthenium, the heteroatom oxygen, and two oxygen atoms of the lacuna are broken, as sometimes happens.^{53–56}

To address such an issue, EXAFS analysis has been carried out. The iminophosphorane derivative **2**, whose structure we know from X-ray diffraction, can be used as a benchmark for the EXAFS study of other compounds of similar structure (Figure 3). Optimization of the parameters requested to simulate the spectrum indicates that the environment of the ruthenium center in **2** is constituted by four Ru–O bonds at 1.96(3) Å, one Ru–O bond at 2.15(6.5) Å, and one Ru–N bond at 1.87(3) Å, in agreement with the distances of 1.962(13) (average value), 2.200(11), and 1.923(16) Å obtained from the X-ray structure. The second shell is found to be constituted by

two tungsten atoms at 3.24(5.2) Å, two tungsten atoms at 3.58(5.3) Å, and two phosphorus atoms at 3.19(3.7) and 3.30(3.7) Å versus 3.302(2) and 3.611(2) Å for the Ru–W distances and 3.199(11) and 3.307(5) Å for the Ru–P distances in the crystal. Further contributions to the Fourier transform of the EXAFS signal could be attributed to tungsten atoms as far off as 6 Å from the ruthenium center.

The EXAFS and Fourier transform signals of **2** and **4** display only a few differences. The first shell of neighbors, albeit similar in overall shape, lies about 0.05 Å further from the ruthenium in **4**, which is consistent with the lower oxidation state of the metal. However, the second shell is almost exactly identical in both cases, validating the hypothesis concerning the presence of the phosphorus-containing ligand as well as the fact that the ruthenium lies completely in the lacuna, with the POM acting as a pentadentate ligand. The environment of the ruthenium, as obtained from the optimization of the simulation of the EXAFS and Fourier transform signals (Figure 4), consists of a first shell of six oxygen atoms [$4 \times 2.01(5.4)$ Å, $1 \times 2.45(6)$ Å, and $1 \times 1.97(5.4)$ Å] and a second shell of four tungsten atoms [$2 \times 3.24(5.5)$ Å and $2 \times 3.57(5.5)$ Å] and two phosphorus atoms [$3.32(5.5)$ Å].

Because **3** cannot be isolated in the solid state, it is impossible to use EXAFS in transmission mode as we did for **2** and **4**. However, thanks to the high intensity of the

(53) Artero, V.; Laurencin, D.; Villanneau, R.; Thouvenot, R.; Herson, P.; Gouzerh, P.; Proust, A. *Inorg. Chem.* **2005**, *44*, 2826–2835.

(54) Laurencin, D.; Villanneau, R.; Gerard, H.; Proust, A. *J. Phys. Chem. A* **2006**, *110*, 6345–6355.

(55) Bi, L.-H.; Kortz, U.; Keita, B.; Nadjo, L. *Dalton Trans.* **2004**, 3184–3190.

(56) Laurencin, D.; Proust, A.; Gérard, H. *Inorg. Chem.* **2008**, *47*, 7888–7893.

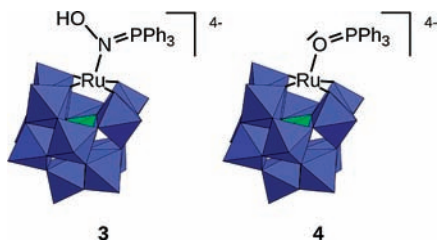


Figure 6. Proposed structures of $[\text{PW}_{11}\text{O}_{39}\text{Ru}^{\text{III}}\{\text{N}(\text{OH})\text{PPh}_3\}]^{4-}$ (**3**) (left) and $[\text{PW}_{11}\text{O}_{39}\text{Ru}^{\text{III}}\{\text{OPPh}_3\}]^{4-}$ (**4**) (right).

X-ray beam at the Soleil synchrotron facility, we were able to work in fluorescence mode on a frozen acetonitrile solution. Despite the relatively high level of noise due to the low ruthenium concentration (4.4 mM, about 400 ppm), the close similitude between the EXAFS data and Fourier transform signals of **3** and **4** point to a parent structure for both compounds. The optimization of the parameters requested to simulate the spectrum indicates the following distances around the ruthenium center: 2.02(6.5) Å ($4 \times \text{Ru}-\text{O}_\text{W}$), 2.48(7.2) Å ($\text{Ru}-\text{O}_\text{P}$), 1.99(6.5) Å ($\text{Ru}-\text{N}$), 3.29(5.3) Å ($2 \times \text{Ru}-\text{W}$), 3.59(5.2) Å ($2 \times \text{Ru}-\text{W}$), 3.20(6.5) Å ($\text{Ru}-\text{P}_\text{Ph}$), 3.36(5.5) Å ($\text{Ru}-\text{P}_\text{O}$) (Figure 5), emphasizing the kinship between **3** and **4**. We can therefore conclude from the XAS data that in both **3** and **4** the lacunary POM $[\text{PW}_{11}\text{O}_{39}]^{7-}$ acts as a pentadentate ligand toward a Ru^{III} center and the sixth ligand is a triphenylphosphine derivative.

Discussion

Structure of Compound 4. Several lines of evidence led us to formulate compound **4** as $[\text{PW}_{11}\text{O}_{39}\text{Ru}^{\text{III}}\{\text{OPPh}_3\}]^{4-}$ and to propose the structure shown in Figure 6. The incorporation of one ruthenium atom in the $[\text{PW}_{11}\text{O}_{39}]^{7-}$ framework is indicated at first by the dark-brown color of the solution, caused by a broad charge-transfer band ($\lambda_{\text{max}} = 360$ nm; $\log \epsilon = 3.9$) and was confirmed by mass spectrometry as well as by the intensity of the X-ray absorption during the XAS experiments. The complete incorporation of the ruthenium in the lacuna ("in-pocket" configuration) is supported by the EXAFS data and by crystallization in a cubic space group.

The oxidation state of the ruthenium was found to be III by XANES (see the previous paragraph), with an edge close to what is observed for $[\text{PW}_{11}\text{O}_{39}\text{Ru}^{\text{III}}\{\text{OH}_2\}]^{4-}$ (**5**). The similarity between the electronic properties of those two compounds is also indicated by the identical positions (albeit with different absorption coefficients) of their charge-transfer band. This, in turn, indicates that the overall charge of those two species is likely to be the same, i.e., that the ruthenium in **4** bears a neutral ligand.

The incorporation of a ligand derived from PPh_3 in **4** is suggested by the observation of two signals in its ^{31}P NMR spectrum (Table 1) and is confirmed by mass spectrometry and ^1H NMR, IR, and Raman spectroscopies. The presence in the IR spectrum of a band at 1112 cm^{-1} , very close to the $\text{P}=\text{N}$ double-bond stretching mode in **2** (1114 cm^{-1}), suggests the presence of a $\text{P}=\text{X}$ bond, where X is either oxygen or nitrogen (discrimination between these two is impossible from mass spectrometry because of the broadness of the peaks generated by the wide isotopic distribution of tungsten). We infer from the electrochemical

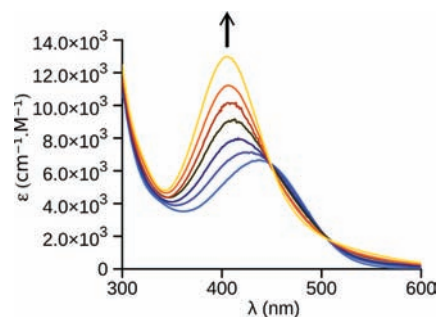


Figure 7. Titration of $[\text{PW}_{11}\text{O}_{39}\text{Ru}^{\text{V}}\{\text{NPPH}_3\}]^{3-}$ (**2**) by OH^- , yielding $[\text{PW}_{11}\text{O}_{39}\text{Ru}^{\text{III}}\{\text{N}(\text{OH})\text{PPh}_3\}]^{4-}$ (**3**).

study that the reduction of the iminophosphorane derivative of Ru^{IV} is very likely centered on the tungsten framework, which rules out a reduced form of **2**. The structure of **4** is thus likely $[\text{PW}_{11}\text{O}_{39}\text{Ru}^{\text{III}}\{\text{OPPh}_3\}]^{4-}$, with the 1112 cm^{-1} IR band assigned to the $\text{P}=\text{O}$ double-bond stretch of the coordinated triphenylphosphine oxide molecule. This value is among the lowest reported for $\text{P}=\text{O}$ stretches in transition-metal complexes of triphenylphosphine oxide: the free ligand displays this band at 1195 cm^{-1} , while the reported values for coordinated molecules are found between 1105^{57} and 1192 cm^{-1} .⁵⁸ This relative weakness of the $\text{P}-\text{O}$ bond suggests, in turn, a strong binding of the ligand to the ruthenium center. As a result, we expect the $\text{Ru}-\text{O}$ distance to be rather short when compared with the metal-oxygen distance in other triphenylphosphine oxide complexes, which lie between 1.9^{59} and 2.5 Å .⁶⁰ Concerning ruthenium, an extended search of the literature yields only a few reports of triphenylphosphine oxide complexes that are fully characterized structurally. Among those, most deal with Ru^{II} derivatives, with $\text{Ru}-\text{O}$ distances ranging from 2.22^{61} to 2.29^{62} Å . As expected, the $\text{Ru}^{\text{III}}-\text{O}$ distance in **4** deduced by EXAFS, 1.97 Å , is significantly shorter. The shortness of the bond between the ruthenium and OPPh_3 , and hence its strength, might be significant in accounting for the stability of compound **4**.

Structure of Compound 3. Because of the instability of **3** in solution and the impossibility of isolating it in the solid state, elucidation of its structure was more difficult. The reaction between **2** and **3** implicates a hydroxide exchange (see above). The resulting formulation of **3** as $[\text{PW}_{11}\text{O}_{39}\text{Ru}^{\text{III}}\{\text{N}(\text{OH})\text{PPh}_3\}]^{4-}$ is also in agreement with mass spectrometry, Raman, and ^1H NMR spectroscopy data, while XANES and EXAFS data underline the structural similarity between **3** and **4**. Next comes the question of the position of the hydroxide fragment. The two most likely possibilities are coordination to the Ru^{V} center or to the nitrogen atom, as illustrated in Figure 6. In the first case, the Ru^{V} center would either become seven-coordinated or

(57) Barral, M. C.; Jiménez-Aparicio, R.; Priego, J. L.; Royer, E. L.; Urbanos, F. A.; Amador, U. *Inorg. Chem.* **1998**, *37*, 1413–1416.

(58) Arnáiz, F. J.; Aguado, R.; Pedrosa, M. R.; De Cian, A.; Fischer, J. *Polyhedron* **2000**, *19*, 2141–2147.

(59) Abdallaoui, H. E. E.; Rubini, P.; Tekely, P.; Bayeut, D.; Lecomte, C. *Polyhedron* **1992**, *11*, 1795–1800.

(60) Cindric, H.; Vrdoljak, V.; Matkovic-Calogovic, D.; Kamenar, D. *Acta Crystallogr., Sect. A* **1996**, *52*, 3016–3018.

(61) Barral, M. C.; Jiménez-Aparicio, R.; Priego, J. L.; Royer, E. C.; Saucedo, M. J.; Urbanos, F. A.; Amador, U. *Polyhedron* **1995**, *14*, 2419–2427.

(62) Li, Y.; Huang, J.-S.; Xu, G.-B.; Zhu, N.; Zhou, Z.-Y.; Che, C.-M.; Wong, K.-Y. *Chem.—Eur. J.* **2004**, *10*, 3486–3502.

adopt an “out-of-pocket” configuration, thus having coordination sites available for the hydroxide. This possibility is supported by the similarities between the UV–visible spectra of **2** and **3**, with charge-transfer bands at 442 and 405 nm, respectively (Figure 7). However, the out-of-pocket configuration can be ruled out from the EXAFS data, which strongly indicate the presence of the “in-pocket” configuration. The second case is akin to a reductive elimination at the ruthenium center, yielding the neutral triphenylphosphine oxime Ph_3PNOH , coordinated through a dative N–Ru bond to the III metallic center. This second scenario, with a nucleophilic attack on the nitrogen, is consistent with the formation of $[\text{Ph}_3\text{PNPPH}_3]^+$ from **2** and is in accordance with both the XANES and EXAFS data. The reduction of ruthenium from Ru^{V} in **2** to Ru^{III} in **3** corresponds to an internal electron transfer within the metal–ligand function, akin to the reduction of Ru^{VI} by PPh_3 addition to the starting nitrido complex **1**.

Compound **3** is, to our knowledge, the first phosphine oxime derivative reported, but it can be related to several parent phosphine imine derivatives such as the *N*-methoxytriphenylphosphinimium cation⁶³ or triphenylphosphinaminoimine.^{64,65} Classical imine derivatives are easily hydrolyzed to the corresponding ketone; thus, it is not surprising that all of the aforementioned species tend to decompose quickly in the presence of water to give triphenylphosphine oxide, a fate from which **3** does not escape. Nevertheless, if care is taken to keep a solution of **3** as devoid of extra hydroxide or water molecules as possible, it can be preserved at room temperature for several minutes. In the absence of better structural data, one can only speculate on the origin of this relative stability. The combination of steric and electrostatic repulsion due to the POM framework is likely to slow down the reaction between **3** and H_2O or OH^- , but some more subtle electronic effect might also be playing a role.

Summary and Conclusion

This study of the reactivity between triphenylphosphine and a ruthenium(VI) nitrido function, embedded in the

lacunary POM $[\text{PW}_{11}\text{O}_{39}]^{7-}$, shows that the reaction proceeds in two well-separated steps. The iminophosphorane derivative $[\text{PW}_{11}\text{O}_{39}\text{Ru}^{\text{V}}\{\text{NPPH}_3\}]^{3-}$ (**2**) that we reported earlier²⁰ is the product of the first, fast step. In the presence of hydroxide, the unstable phosphine oxime complex $[\text{PW}_{11}\text{O}_{39}\text{Ru}^{\text{III}}\{\text{N}(\text{OH})\text{PPh}_3\}]^{4-}$ (**3**) can also form, emphasizing the necessity of careful control of the acid–base conditions even if only a small amount of water is present, which is almost unavoidable in acetonitrile. Compound **3** will then cleanly convert to $[\text{PW}_{11}\text{O}_{39}\text{Ru}^{\text{III}}\{\text{OPPh}_3\}]^{4-}$ (**4**). Compound **2** reacts with a second equiv of triphenylphosphine in a subsequent, slower step to yield the bis(triphenylphosphane)iminium cation $[\text{Ph}_3\text{PNPPH}_3]^+$ and $[\text{PW}_{11}\text{O}_{39}\text{Ru}^{\text{III}}\{\text{OH}_2\}]^{4-}$, thus achieving complete transfer of the nitrogen atom from the POM to the organic substrate. We thus provide some unprecedented insight into the reactivity of a ruthenium iminophosphorane function, in the distinctive environment of the POM.

In the course of this investigation, we characterized two new ruthenium derivatives, $[\text{PW}_{11}\text{O}_{39}\text{Ru}^{\text{III}}\{\text{N}(\text{OH})\text{PPh}_3\}]^{4-}$ (**3**) and $[\text{PW}_{11}\text{O}_{39}\text{Ru}^{\text{III}}\{\text{OPPh}_3\}]^{4-}$ (**4**). With the structural characterization of those two compounds by X-ray diffraction being impossible, we had to resort to several other techniques including XANES and EXAFS, mass spectrometry, ^1H and ^{31}P NMR, UV–visible, IR, and Raman spectroscopies to identify them. Ultimate identification was only possible with the help of thoroughly characterized references such as $[\text{PW}_{11}\text{O}_{39}\text{Ru}^{\text{VI}}\text{N}]^{4-}$ (**1**), $[\text{PW}_{11}\text{O}_{39}\text{Ru}^{\text{V}}\{\text{NPPH}_3\}]^{3-}$ (**2**), and $[\text{PW}_{11}\text{O}_{39}\text{Ru}^{\text{III}}\{\text{OH}_2\}]^{4-}$ (**5**). In the course of this work, we have accumulated spectroscopic data on all of those species. Together with Rong and Pope's study²⁴ as well as others from our laboratory,^{15,20} this study makes the $[\text{PW}_{11}\text{O}_{39}\text{RuL}]^{n-}$ system the most extensively investigated of all ruthenium-substituted polyoxotungstates, with oxidation states of the ruthenium center ranging from II to VI, both in water and in acetonitrile. As such, it might prove to be a useful reference for further studies of ruthenium-containing POMs, a subject that is likely to attract much interest in the near future.^{17–19,66}

Acknowledgment. The present research is supported by Grant ANR-06-BLAN-0249-01 (to A.P.) and by the U.S. Department of Energy Grant DE-FG02-03ER15461 (to C.L.H.).

(63) Rudchenko, V. F.; Ignatov, S. M.; Kostyanovsky, R. G. *J. Chem. Soc., Chem. Commun.* **1990**, 261–262.

(64) Zimmer, H.; Singh, G. *J. Org. Chem.* **1964**, *29*, 1579–1581.

(65) Walker, C. C.; Schechter, H. *Tetrahedron Lett.* **1965**, *20*, 1447–1452.

(66) Howells, A. R.; Sankarraj, A.; Shannon, C. *J. Am. Chem. Soc.* **2004**, *126*, 12258–12259.